J Nanostruct 15(4): 1642-1660, Autumn 2025

RESEARCH PAPER

Fabrication and Characterization of a Graphene Oxide-Reinforced Hydrogel Biocomposite Loaded With A-Lipoic Acid and Icariin-Based Nanocarriers: A Pilot Preparative Study

*Aqeel Akab Sarhan *, Ismaeil Haririan, Mohammed Akrami*

Department of Pharmaceutics, School of Pharmacy, Tehran University of Medical Sciences, Tehran, Iran

ARTICLE INFO

Article History:
Received 25 June 2025
Accepted 16 August 2025
Published 01 October 2025

Keywords:
α-lipoic acid; icariin
Biomaterials; gelatin
Graphene oxide
Methylcellulose
Scaffold hydrogel
Sodium alginate

ABSTRACT

Fabricated drug-loaded hydrogels are versatile biomaterials with significant applications in bone tissue engineering, capable of mimicking the natural extracellular matrix (ECM) and providing controlled drug delivery essential for promoting bone regeneration and repair. This study developed a hydrogel biocomposite from natural biomaterials including gelatin, sodium alginate, and methylcellulose, combined with nanocarriers loaded with alpha-lipoic acid (ALA) and icariin to enhance bone tissue regeneration. The optimal hydrogel biocomposite composition consisted of methylcellulose (4%), gelatin (12%), and sodium alginate (6%), demonstrating adequate viscosity, controlled extrusion, shape retention, and enhanced mechanical stability, with 0.5% graphene oxide incorporation significantly improving the moduli G'/G", complex viscosity, and viscoelastic properties. ALA-loaded TPGs micelles exhibited spherical nanoparticles (20-40 nm diameter), -1.9 mV surface charge, 70% encapsulation efficiency, sustained 48-hour release (85.9±2.5%), and 85% hMSCs cell viability at 6.25-12.5% concentration, while icariin-loaded PLGA nanoparticles showed spherical morphology (469.1 nm diameter, 0.234 PDI), -1.2 mV surface charge, 7.0±0.4% drug loading content, sustained seven-day release (74.8±1.7%), and high cell viability (89.7-99.05%) at tested concentrations. The optimal size distribution, favorable surface charge, and sustained drug release profiles of both nano-formulations demonstrate their appropriateness for bone tissue engineering applications, confirming that the fabricated hydrogel composite with drug-loaded nanocarriers provides an effective platform for targeted, prolonged delivery of osteo-regenerative agents, enhancing bone regeneration and repair.

How to cite this article
Sarhan A., Haririan I., Akrami M. Fabrication and Characterization of a Graphene Oxide-Reinforced Hydrogel Biocomposite Loaded With A-Lipoic Acid and Icariin-Based Nanocarriers: A Pilot Preparative Study. J Nanostruct, 2025; 15(4):1642-1660.
DOI: 10.22052/JNS.2025.04.013

INTRODUCTION

Drug-loaded fabricated hydrogels biocomposite are considered as promising multifaceted platforms integrating biological signals, structural support, and controlled therapeutic delivery to hasten and boost the repair of bone defects [1-4]. These biocomposite formulations have numerous applications such as a) localized drug delivery like growth factors [1], antibiotics, anti-inflammatory drugs [5, 6], angiogenic factors [7], b) scaffolds for

* *Corresponding Author Email: phar.aqeel@yahoo.com*

encapsulation and drug delivery, c) filling irregular bone defects [8], d) controlled release kinetics, and e) responsive drug delivery [9].

Hydrogel scaffolds synthesized for tissue engineering purposes are classically categorized with regard to their composition into three groups: natural, synthetic [10], and hybrid [9]. Natural hydrogels (gelatin, collagen, or alginate) are extremely biocompatible and imitate the native extracellular matrix (ECM) *in vivo*. Synthetic hydrogels (poly (lactic-co-glycolic acid) (PLGA) or polyethylene glycol (PEG)) display fined -tuned mechanical properties accompanied with foreseeable rates of biodegradation. Combined features of synthetic and natural hydrogels were integrated in the last hydrogel type namely hybrid hydrogels to compromise between the biological and mechanical properties. Graphene oxide (GO) is broadly combined with hydrogels to synthesize biocomposite materials with meaningfully boosted biological, mechanical, and stability properties. Meanwhile, GO-incorporated hydrogels biocomposite show bioactive surface, promoting cell adhesion, cell proliferation, and cell differentiation. The consequential GO- based hydrogel biocomposites are extremely appropriate and well-copied with numerous tissue engineering applications, particularly in bone regeneration [11-13].

The amphiphilic polymer D-α-tocopheryl polyethylene glycol 1000 succinate forms the TPGs nanocarriers. These anaocarriers are chacterized with excellent bioompatability and good capability to generate stable micelles. Consequently, they are being exploited as efficient drug delivery systems [7]. The universal antioxidant, antiinflammatory, and free radical neutralizer α-lipoic acid (ALA), in both aquious and lipoic environments, display significant therapeutic potential, mostly in handling conditions such as diabetic neuropathy [14]. Despite its high therapeutic potential, low bioavaialbility and poor aquoeus solubility halt its usage. Hence, ALA-loaded TPGS nanocarriers are considered a gold solution to overcome these undesired criteria. The encapsultion of ALA within TPGs would result in high ALA laoding capacity, prolonged drug release with a high guaranteed of arrival to the target site, and boosted antioxidant ALA in numerous applications particualry tissue regernation [15]. Despite the promising osteoinductive properties of icariin, a natural flavonoid of plant origin, its poor solubility in aqueous environment and low bioavailability greatly restrict its exploitation in the medical field. This would necessitate the indispensable need to encapsulate icariin in excellent drug nanocarriers-based sytsems like poly(lactic-co-glycolic acid) (PLGA). The encapsulation of icariin within PLGA nanocarriers would add valuable properties to icariin such as sustained release, improved solubility, boosted stability, and improved targeted therapeutic efficacy. As a consequence, the well-controlled icariin delivery would reinforce bone regeneration and enhance osteogenic differentiation [16, 17]. In this context, the goal of the present study is to fabricate and characterize graphene oxide-reinforced hydrogel biocomposite loaded with α-lipoic acid and icariin-based nanocarriers. This work is regarded as a pilot preparative study for conducting a scaffold 3D bioprinting for bone tissue engineering purposes in a prospective study.

MATERIALS AND METHODS

Materials and reagents

The following materials were used: dialysis bags (14 kDa and 12 kDa cut-off, Sigma-Aldrich), icariin (98% purity, China), D-α-tocopherol polyethylene glycol 1000 succinate (TPGS, BASF), absolute ethanol (HPLC-grade, Merck), acetonitrile (HPLC-grade, Merck), acetic acid (glacial, Sigma-Aldrich), deionized water (DI, Milli-Q), phosphate-buffered saline (PBS, pH 7.4, Gibco), Dulbecco's Modified Eagle's Medium (DMEM, Gibco), gelatin (Type A, 300 bloom, Sigma-Aldrich), collagenase IV (Gibco), α-lipoic acid (ALA, ≥99%, Sigma-Aldrich), fetal bovine serum (FBS, Gibco), penicillin-streptomycin (10,000 U/mL, Gibco), Sudan Black solution (SB, Sigma-Aldrich), 2.5% glutaraldehyde solution (Electron Microscopy Sciences), 10% neutral buffered formalin (Sigma-Aldrich), hexamethyldisilazane (HMDS, Sigma-Aldrich), 0.1% Triton X-100 (Sigma-Aldrich), 8% FBS solution (prepared from Gibco FBS), Alexa Fluor 488 (Thermo Fisher Scientific), Alamar Blue reagent (Thermo Fisher Scientific), Alkaline Phosphatase Kit (ALP, Sigma-Aldrich), Tween 20 (Sigma-Aldrich), primers for osteocalcin (OCN), runt-related transcription factor 2 (RUNX2), and osteopontin (OPN) (custom-synthesized, Integrated DNA Technologies), Trizol reagent (Invitrogen), HieffTM qPCR SYBR Green Master Mix Kit (Yeasen), MTT (3-(4,5-dimethylthiazol-2-yl)-2,5-diphenyltetrazolium bromide, Sigma-Aldrich),

isopropanol (HPLC-grade, Merck), sodium citrate monobasic (Sigma-Aldrich), glycerol (Sigma-Aldrich), methylcellulose (MC, 4000 cP, Sigma-Aldrich), sodium alginate (medium viscosity, Sigma-Aldrich), graphene oxide (GO, 2 mg/mL dispersion, Graphene), poly(lactic-co-glycolic acid) (PLGA, MW 24,000–38,000 Da, 50:50 lactide: glycolide, Sigma-Aldrich), and poly(vinyl alcohol) (PVA, MW 31,000 Da, 87–89% hydrolyzed, Sigma-Aldrich).

Preparation of graphene oxide incorporated hydrogel composite ink

The composite ink consists of three biopolymers gelatin, sodium alginate, methylcellulose, and graphene oxide. The preparation of graphene oxide incorporated hydrogel composite ink is a multistep sequential process as illustrated in Fig. 1.

Preparation of hydrogel composite of three biopolymers solutions

Five distinctive formulations of the three biopolymers, each 10 ml, were prepared by mixing varying concentrations of each biopolymer. Each formulation was prepared according to the recipe outlined in Table 1. For instance, formulation number I consisted of three solutions. Solution A was prepared by dissolving MC in 3.33 mL cold deionized water (4°C), while solution B was prepared by dissolving gelatin in 3.33 mL warm deionized water maintained at 40 °C. Solution C was prepared by dissolving SA in 3.33 mL deionized water maintained at room temperature. Then, three solutions A, B, and C were combined altogether under constant stirring at 25 °C to halt the development of air bubbles and ensure even homogenization. Post mixing, each formulation had been subjected to continuous stirring for

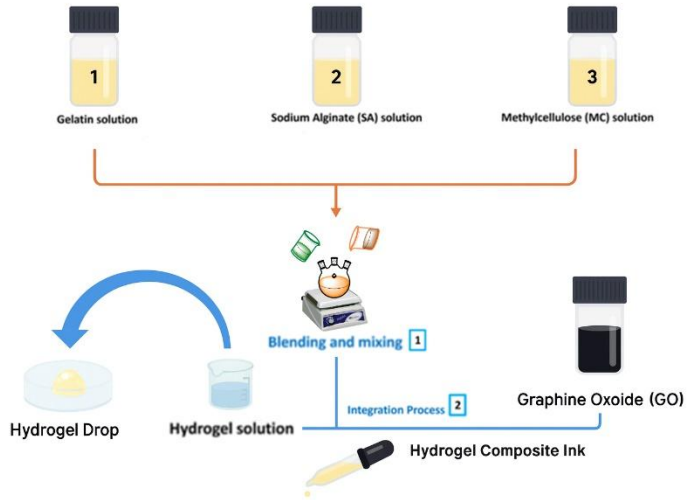

Fig. 1. A flowchart elucidating the sequential steps involved in the preparation of graphene oxide incorporated- hydrogel composite ink.

Table 1. Hydrogel composite (Inks formulations).

Ink Formulation #	Methylcellulose %(w/v)	Gelatin %(w/v)	Sodium Alginate %(w/v)
I	3	5	5
II	4	7	7
III	4	10	10
IV	4	12	6
V	7	2.5	2.5

30 min and were stored at 4 °C for 24 hours to permit full hydration and stabilization of the polymer networks. The hydrogel composite of three biopolymers is synonymously recognized as the inks composite. The inks formulations were equilibrated to room temperature and gently homogenized preceding their usage. Moreover, the inks formulations were subjected to pH adjustment to pH of the ink formulations to 7.4 ± 0.2, sterile filtration through a bacterial filter 0.22 µm filter and visual check to verify their homogeneity and lack of any undissolved particles [18].

Printability assessment of hydrogel composite ink

The printability of the hydrogel composite ink was assessed using an extrusion-based protocol with a 3D bioprinter (PAS, Iran). Shortly, a 10 mL syringe was filled with the formulation ink. Extrusion tests were performed at 25 ± 2°C at a constant flow rate of 0.5 mL/min, dropping 5 mL of ink on a glass substrate to generate continuous filaments. Printability was evaluated considering certain criteria like (i) uniformity of the formed filaments, (ii) extrudability, (iii) figure retention post-extrusion, and (iv) integrity of the formed filaments. Filaments were placed as 5 cm straight lines on a glass substrate, and figure retention was monitored for along 5 min [19].

Preparation of graphene oxide solution

A solution of graphene oxide (GO) at a concentration of 2 mg/mL was prepared by dispersing the GO in deionized water using sonicator probe (Sonics Vibra-Cell, USA, 130 W, 20 kHz, 6 mm probe) for 2 hours at 40% amplitude, with 30 sec cycle on/ off pulse cycle in an ice bath to reduce heat generation. The GO suspension was centrifuged at 4,000 rpm for 15 min to get rid of any impurities. Then, the GO supernatant was gathered and kept for next use [20].

Integration of GO solution into hydrogel composite ink

GO-incorporated hydrogel composite ink was prepared by mixing the GO suspension with cold deionized water (4 °C). Then the three biopolymers were added to the GO solution in the following order under stirring: MC, cooled gelatin solution previously dissolved in warm deionized water (40 °C), and dissolved SA, respectively. Again, the whole process was conducted under stirring to prepare homogenous solution [21]. The best hydrogel composite ink formulation settled in Table 1 was used to prepare three GO-incorporated hydrogel composite ink. The three GO-incorporated hydrogel composite inks involved three GO concentrations 0.1%, 0.5%, and 1% (w/v) [22]. The three GO-incorporated hydrogel composite inks were homogenized by mechanical homogenizer (IKA T25) at 500 rpm for 30 min to ensure air bubbles removal. Moreover, pH adjustment to 7.4 ± 0.2 to ensure the biocompatibility. The inks were kept at 4°C for 24 hours for stabilization purposes. The homogeneity of the GO-incorporated hydrogel composite inks were ascertained by visual inspection and microscopic examination to guaranteed suitability for further applications [23].

Rheological characterization of GO incorporated hydrogel composite ink

Rheological characterization of the GO-incorporated bioinks was conducted using an Anton Paar MCR300 rheometer (SN634038; FW2.20). Frequency sweep tests were performed to assess the viscoelastic properties of GO-incorporated bioinks at different GO concentrations 0.1, 0.5, and 1%(w/v). The tests were conducted within the linear viscoelastic region at a fixed strain amplitude of 1%. The flow properties of the GO-incorporated bioinks were assessed using controlled shear rate tests. The measurements were conducted by applying a logarithmically increasing shear rate from 0.1 to 1000 s^{-1}, with 60 measurement points and a point duration of 3 sec [24, 25].

Preparation of α-Lipoic Acid-loaded TPGS micelles

Alpha-lipoic acid (ALA)-loaded D-α-tocopheryl polyethylene glycol succinate (TPGS) micelles were synthesized using a modified solvent evaporation technique, initiated by dissolving 150 mg of TPGS and 5 mg of ALA in 10 mL of HPLC-grade methanol with magnetic stirring at 300 rpm for 30 min at 25 °C. The solvent was evaporated at 40 °C using a rotary evaporator (at 100 rpm) to create a thin film, which was then freeze-dried for 30 min to eliminate any remaining solvent. To form micelles, the film was re-hydrated with 15 mL of PBS (pH 7.4) and stirred magnetically at 200 rpm for 48 hours. The resulting suspension was then filtered through a 0.22µm cellulose acetate membrane

and kept in amber vials at 4 ∘C.

Characterization of ALA-loaded TPGs micelles
Drug Loading Determination

A validated HPLC method was applied to determine the drug loading content and encapsulation efficiency of α-lipoic acid in TPGS micelles. Concisely, 1 mg of lyophilized ALA-loaded TPGS micelles was allowed to dissolve in 1 mL HPLC -grade methanol followed by continuous agitation for 300 rpm for 2 hours. Then, the solution was filtered through 0.22-µm PTFE syringe filter to get rid of any potential particulates. A volume of 20 µL of the filtered solution was injected into the HPLC C18 reverse -phase column, at a flow rate of 1.0 mL/min, at 35 °C, with an isocratic elution using a mobile phase of 60% acetonitrile and 40% potassium dihydrogen phosphate buffer (50 mM, pH 3.5). The detection wavelength for ALA was 320 nm [26].

In vitro drug release

The rate at which α-lipoic acid (ALA) was released from TPGS micelles was studied using a dialysis membrane method. This experiment was conducted in conditions similar to those found in the body. To begin, 5 mL of the ALA-containing TPGS micelle solution was put into a dialysis bag (with a molecular weight cutoff of 14,000 Da), which was then securely sealed at both termini. Then this dialysis bag was placed into a beaker holding 20 mL of a release solution (phosphate-buffered saline at pH 7.4, with 1% Tween 20). The setup used a 1:4 ratio of the solution inside the dialysis bag (donner solution) to the solution outside (receptor compartment solution) it. At specific times, 1 mL samples were withdrawn from the external release solution and further analyzed using a previously validated HPLC method as mentioned above. To keep the volume constant, 1 mL of fresh release medium was added back each time a sample was withdrawn.

Size distribution and Zeta potential analysis

Dynamic light scattering (DLS) instrument quipped with a633 nm He-NE laser operating at 4 mW power was used to determine the size distribution and zeta potential measurements. For size measurements, the micellar suspension was diluted with filtered (0.22 µm) ultrapure water to achieve an optimal scattering intensity. The measurements were conducted at a fixed scattering angle of 173° (backscatter detection) and a temperature of 25 °C. Similarly, the sample of micellular suspension was prepared with the same manner for zeta potential measurements and then transferred to a specialized electrophoretic cell. The measurements were performed using phase analysis light scattering (PALS) at 25°C.

Transmission electron microscope (TEM) analysis

A single drop of the freshly prepared micellar suspension was placed copper grids coated with carbon for 5 minutes at room temperature (25°C), stained with 2% uranyl acetate for 2 minutes, and air-dried for 15 minutes. Then images were taken at various magnifications.

Fourier Transform Infrared Spectroscopy (FTIR) analysis

The FTIR analysis was conducted for three structures: pure α-lipoic, and pure TPGS and the formulated nanoparticle. Each sample was cautiously positioned on the diamond ATR crystal and crushed with KBr using the pressure clamp to guarantee optimal contact. The applied wavelength spectrum was (4000-400 cm^{-1}, 4 cm^{-1}resolution, 64 scans) for each tested sample to augmnet the signal-to-noise ratio. The sample chamber was purged with dry nitrogen gas throughout the analysis to reduce atmospheric interference.

Preparation of Icariin-loaded PLGA nanoparticles

The modified oil-in-water (O/W) emulsion solvent evaporation method was used to synthesize icariin-loaded poly (lactic-co-glycolic acid) (PLGA) nanoparticles. The organic phase consisted of 62.5 mg PLGA (MW: 24,000–38,000 Da, 50:50 lactide: glycolide) and 5 mg icariin in 5 mL solvent (dichloromethane: methanol (1:1 v/v)). However, the aqueous phase was 50 mL of 1% (w/v) polyvinyl alcohol (87–89% hydrolyzed). Step-wisely, the organic phase was added to the aqueous phase with sonication (Sonics Vibra-Cell VCX130, 70% amplitude, 6 mm probe) for 5 minutes in an ice bath to halt thermal degradation. Finally, the formed emulsion was stirred at 150 rpm for 10 hours at 22 ± 2°C to help evaporate solvents and form hardened icariin-loaded PLGA nanoparticles [27].

In vitro drug loading

Icariin loading and encapsulation efficiency

in icariin-loaded PLGA nanoparticles were determined using HPLC (a C18 column of 150 mm × 4.6 mm, 5 µm, a mobile phase of acetonitrile: 50 mM potassium dihydrogen phosphate (60:40 v/v, pH 3.5) at 1.0 mL/min at 35 °C). The UV-vis detector was used at 350 nm. A 1 mL icariin-loaded PLGA nanoparticles emulsion was added to 1 mL PBS (pH 7.4) with agitated at 300 rpm for 6 hours. Then, the mixture was filtered (0.22 µm). Then 20 µL of the previously mentioned mixture (sample) was injected into the C18 column.

In vitro drug release

The release of icariin from icariin-loaded PLGA nanoparticles was appraised using a dialysis bag (12 kDa cut-off). Shortly, 1 mL of icariin-loaded PLGA nanoparticles suspension was transferred to the dialysis membrane soaked in 10 mL of dialysis buffer (PBS, pH 7.4 with 1% (w/v) Tween 80) to guarantee sinking. The release of icariin from icariin-loaded PLGA nanoparticles was monitored at 37±0.5 °C with gentle stirring at 100 rpm. One mL samples were withdrawn at the indicated time intervals (0, 2, 4, 8, 12, 24, 48, 72, 96, 120, 144, and 168 hours) and replaced with an equal volume of fresh release medium. The amount of released drug was quantified using the previously validated HPLC method [28].

Scanning Electron Microscopy (SEM) analysis

The surface morphology and particle size of Icariin-loaded PLGA nanoparticles surface morphology and size were examined using SEM [29, 30]. Concisely, a droplet of icariin from icariin-loaded PLGA nanoparticles emulsion was laid on a clean silicon wafer and left to air-dry at room temperature. Then, the sample was sputter-coated with a thin layer of gold under vacuum. Imaging under SEM was picked using a field emission scanning electron microscope operating at 5 kV with high vacuum conditions.

FTIR analysis of Icariin Loaded PLGA nanoparticles

The chemical composition of three structures and the potential interactions in between PLGA, icariin, and the formulated nanoparticles were unveiled using FTIR at 25 ±2°C. The samples were crushed by grinding with spectroscopic grade KBr powder and compressed into transparent pellets. The applied wavelength spectrum was (4000-400 cm^{-1}, 4 cm^{-1}resolution, 32 scans) for each tested sample to elevate the signal-to-noise ratio.

DLS and Zeta Potential Examination of PLGA nanoparticles

The hydrodynamic diameter, poly dispersity index (PDI), and zeta potential of the icariin-loaded PLGA nanoparticles were measured using a Malvern Zetasizer NanoZ analyzer (Malvern Instruments, UK) according to a previously reported procedure [31].

MTT assay

The cytotoxicity assessment for ALA-loaded TPGs micelles and icariin loaded PLGA nanoparticles were conducted on (3-(4,5-dimethylthiazol-2-yl)-2,5-diphenyltetrazolium bromide) assay on human mesenchymal stem cells (hMSCs). Culturing of hMSCs was conducted in Dulbecco's Modified Eagle Medium (DMEM) supplemented with 10% fetal bovine serum (FBS) and 1% penicillin-streptomycin at 37 °C in a carbon dioxide humidified incubator. The hMSCs were seeded in 96 -well plates at a density of 1 × 10^4 cells per well and permitted to stick (adhere) to the wells bottom for 24 hours. Then, the cells were treated with various concentrations of α-ALA- loaded TPGS micelles and icariin Loaded PLGA nanoparticles emulsion (100, 50, 25, 12.5, and 6.25% of the stock solution) separately. A control group was prepared as untreated cells. Post 24 hours of treatment, 20 µL of MTT solution (5 mg/mL in PBS) was added to each well followed by further incubation to additional 4 hours at 37 °C. Removal of the medium was performed after the 4 hours incubation period. Then, the formed formazan crystals were dissolved in 100 µL of DMSO and the absorbance was measured at 570 nm using a microplate reader (Model, Manufacturer). Cell viability was calculated as a percentage relative to the untreated control cells. All experiments were performed in triplicate.

RESULTS AND DISCUSSION

Printability Assessment

One out of five bioink formulations settled in Table 1 exhibited its superiority as a printable bioink. This bioink formulation was designated IV, with the following composition in terms of % (w/v): 4.0 MC, 12.0 gelatin, and 6.0 SA. These superior printability criteria could be attributed to the high gelatin content relative to the moderate content of MC and SA. The high content of gelatin (12%) would provide enhanced mechanical properties appropriate for both soft and hard tissue

engineering purposes. The moderate content of MC (4%) helps maintain the adequate viscosity required to guarantee good flow characteristics. While, this moderate SA concentration (6%) did prove to be crucial issue for maintaining optimal crosslinking density meanwhile facilitating proper flow characteristics. In stark contrast, the remaining ink formulations I-III, and V displayed unpreferable printable characteristics such as insufficient mechanical strength post extrusion exemplified by bioink formulations I-III with lower gelation content, excessive viscosity and difficult flow criteria as a consequence of high content of MC (7%) exemplified by bioink formulation V, inadequacy in shape fidelity and limited cross-linking potential exemplified by bioink formulations I-III and V, respectively. Whilst, the optimized compositing of bioink formulation IV did succeed to impose preferable printable criteria like ideal viscosity with controlled extrusion and shape retention, enhanced mechanical stability with higher gelatin content, well-balanced cross-linking density as a result of a proper SA concentration, and well-consistent filament formation with excellent structural integrity. Present finding is in a good agreement with a previous finding stated that the elevated gel concentration would improve construct stability and cell adhesin properties [32].

Rheological Properties of GO-Incorporated Bioinks
Frequency Sweep Analysis

The frequency sweep tests did provide full perceptions into the viscoelastic performance of the GO-incorporated bioinks at different GO concentrations (0.1%, 0.5%, and 1% w/v). The storage modulus (G'), loss modulus (G"),

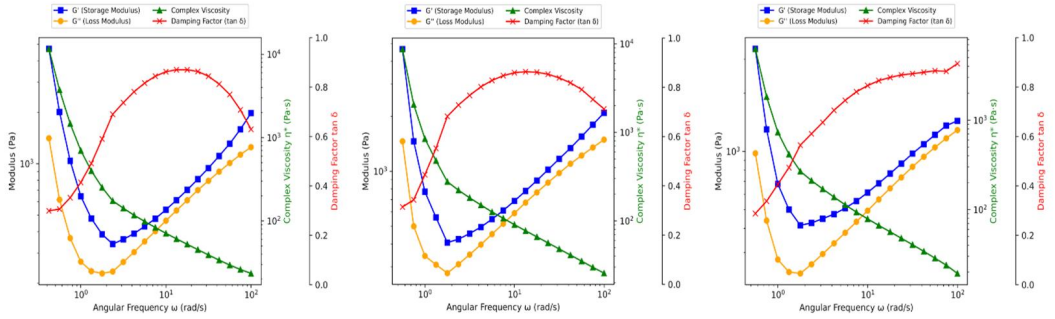

Fig. 2. Frequency Sweep Analysis of GO-Incorporated Bioinks at different GO concentrations (0.1%, 0.5%, and 1% from left to the right, respectively).

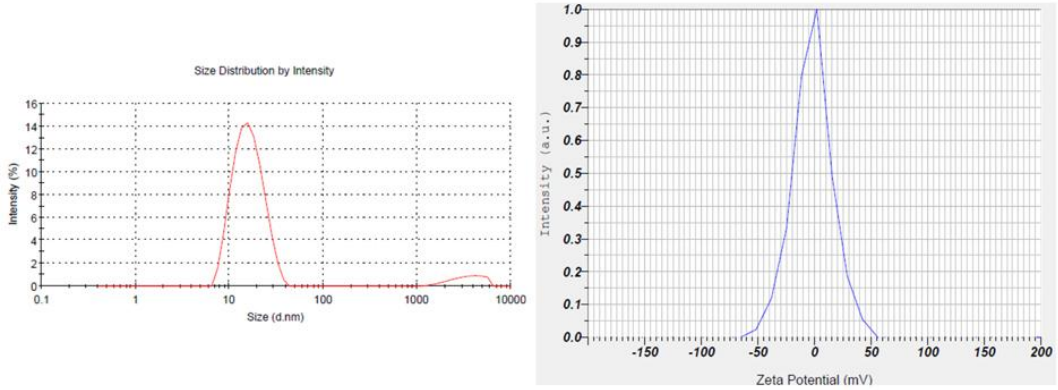

Fig. 3. Size distribution intensity plot by dynamic light scattering (DLS) (A) and Zeta potential distribution curve (B) of ALA-TPGS micelles.

complex viscosity (η*), and damping factor (tan δ) as functions of angular frequency for all three formulations were displayed in Fig. 2. As shown in Fig. 2, all GO-incorporated bioinks displayed a dominant gel-like performance, with the storage modulus (G') steadily surpassing the loss modulus (G") across the studied frequencies (0.1-100 rad/s), corroborative stable 3D network construction [33]. This would in turn maintain shape fidelity after extrusion [34]. Both moduli increased with frequency, a typical hydrogel property. At 0.5% GO, the bioink formulation did exhibit the highest stiffness, signifying an optimal GO concentration for exploiting mechanical stability. Conversely, at elevated GO concentrations, stiffness might reduce as a consequence of agglomeration, weakening the network [35]. Regarding complex viscosity (η*), all bioink formulations shown in Fig. 2, demonstrated shear-thinning behavior, a valuable stuff for extrusion-based bioprinting, with η* diminishing as frequency augmented. This performance tracks the Cox-Merz rule, pinpointing robust shear-thinning characteristics that are gainful for extrusion-based bioprinting [36]. The 0.5% GO-incorporated bioink formulation displayed the highest η*, making parallel with its greater elasticity. The damping factor (tan δ = G"/G') for all bioink formulations in Fig. 2 demonstrated a major elastic behavior at low frequencies, shifting towards an enhanced viscous contribution at higher frequencies [37]. The damping factor (tan δ = G"/G') delivers valuable information concerning the relation contribution of viscous and elastic components. At higher GO concentrations (Fig. 2), the bioinks showed increased viscous behavior, potentially due to GO's lubricating effect or network disruption [38]. Whereas, all bioink formulations (Fig. 2) did demonstrate structural reorganization and yield stress at low frequencies, vital for keeping printed shape. At 0.5% GO-incorporated bioink formulation, the most optimal and balanced viscoelastic properties were obtained (Fig. 2), underpinning its high appropriateness bioprinting with high resolution and excellent shape fidelity [39].

At most the incorporation of GO in bioinks formulations would strengthen the H-bonding, physical entanglements, π-π stacking, and electrostatic interactions in the polymer network, reinforcing robust mechanical properties. In stark contradict, increasing the GO concentration beyond 0.5% would impose adverse consequences in terms of non-uniform distribution of GO sheets

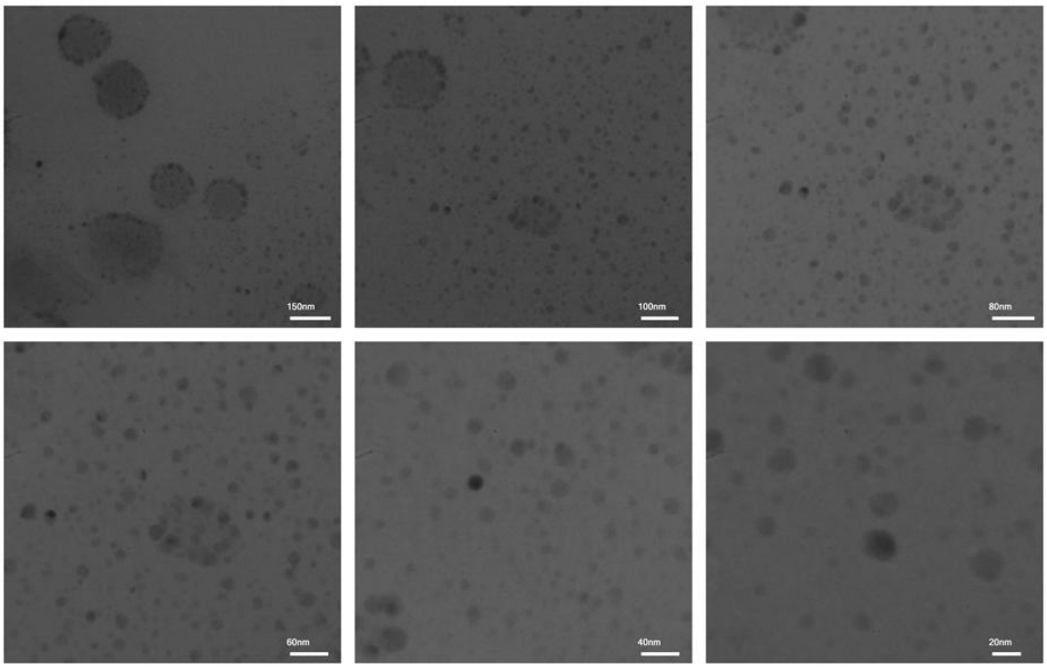

Fig. 4. TEM images of ALA- loaded TPGS micelles at different scale bars of 150, 100, 80, 60, 40, and 20 nm.

with compromised mechanical and viscoelastic properties. Thus, the rheological properties of the bioinks formulation provide good insights about the tailored bioinks formulations to meet peculiar demands for exploitation in certain tissue engineering applications.

Characteristics of ALA-TPGS Micelles

DLS and zeta potential pattern analysis

The DLS measurements elucidated a monomodal size distribution with an average hydrodynamic diameter around 30-40 nm (Fig. 3A), which is localized within the optimum range reported to fit the application concerned with drug delivery [40]. Moreover, the sharp peak portrayed in Fig. 3A reveals arrow size distribution, underpins satisfactory synthesis of uniform micelles characterized by low polydispersity. This size range is positioned within the window 20-200 nm, which is preferable to avoid quick renal clearance though keeping the capability to penetrate biological barriers. This noted size range is well- consistent with previous reports of TPGS-based micellar systems, as the amphiphilic nature of TPGS helps encourage the self-assembly into nano-sized based structures.

The measurements of zeta potential exhibited a peak value around -1.9 mV, as indicated by the symmetrical distribution curve (Fig. 3B). The obtained negative surface charge is symbolic of good colloidal stability, where the particles displaying values of absolute zeta potential around 0 mV and negative characteristically demonstrate adequate electrostatic repulsion to halt the formation of aggregates [36]. The reason underlying the presence of negative charge can be ascribed to the terminal -OH groups of the TPGS molecules positioned at the surface of these micelles [41]. This surface criterion is mostly advantageous for biological applications, because it reinforces enhanced cellular interactions though keeping stability under physiological conditions. Hence, the present ALA-TPGS micelles are characterized by optimal size distribution and favorable surface charge, that underpin the appropriateness of these micelles for drug delivery applications.

Morphological Analysis by TEM

The morphological characteristics of ALA-loaded TPGS micelles were broadly examined using TEM, with images taken at multiple magnifications ranging from 20 -150 nm scale bars (Fig. 4). Spherical, well-defined nanostructures with The TEM micrographs reveal spherical, well-defined nanostructures with a quite even size distribution, emphasizing the satisfactory development of micellar assemblies. The spherical appearance of ALA-loaded TPGS micelles would guarantee reduced surface area to volume ratio along with diminished opsonization, that is gainful for drug delivery applications. Obviously, the marked spherical appearance of ALA-loaded TPGs micelles is in a good accordance with the self-assembly attitude developed by TPGs molecules, where the hydrophobic nature of vitamin E reinforce its positioning in the internal space for drug encapsulation whilst the PEG chains remain

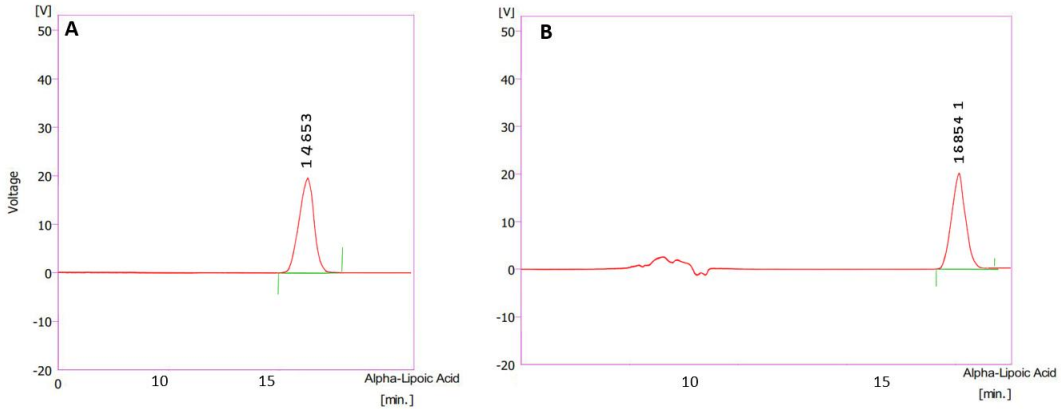

Fig. 5. HPLC chromatographic analysis peaks for ALA standard (A) and the drug (ALA)-loaded TPGs formulation (B).

in the outer corona. Additionally, the darker region of the spherical nanoparticles surrounded by a lighter peripheral layer would ascertain the successful assembly of ALA-loaded TPGs with ALA, with hydrophobic nature, incorporation into the center region of the micelles. The contrast variance between the core and shell regions can be assigned to the discrepancy in the electron density of the vitamin E core comprising the drug and the hydrous PEG halo.

Regarding the particle size, TEM revealed that ALA-loaded TPGs micelles showed a size localized in the range from 20-40 nm, where at most particles size demonstrate a range from 20-30 nm. Again, this size range guaranteed no rapid renal clearance, though still being small enough to halt recognition by the reticuloendothelial system (< 200 nm). Present finding of particle size range is in a partial agreement with a previous finding stating TPGs-based nanocarriers with a size range from 40-70 nm [42]. Notably, the absence of substantial aggregation in the TEM images would reflect the good colloidal stability of the micellular system which is assigned to the efficacious stearic hindrance provided by PEG on the micellular chains preventing the inter-particle interactions and aggregation [43].

Drug loading profile

ALA loaded on TPGs micelles was successfully quantified using a validated HPLC method, where ALA incorporated in the TPGs micelles was detection after a retention time of 15.4 minutes (Fig. 5B) quite similar to the retention time required for detection of the standard ALA (Fig. 5A). The peaks deciphered in the chromatogram settled in Fig. 5 showed good selectivity and resolution. This analysis exhibited outstanding analytical accuracy with negligeable interference, validating the positive drug loading and the method's robustness for complex micellar systems. The validated HPLC method for ALA showed extraordinary analytical presentation, demonstrating perfect linearity (R^2 > 0.999), high accuracy (RSD < 2%), and accurate recovery (98-102%). Its high sensitivity (LOD: 0.1 µg/mL, LOQ: 0.3 µg/mL) and ideal chromatographic separation emphasize consistent and precise quantification within pharmaceutical formulations [44].

The encapsulation efficiency is defined as the percentage of the drug encapsulated or entrapped or adsorbed in/on the nanocarrier. The encapsulation efficiency for ALA in the TPGs micellular system was determined to be around 70%, which is higher than that of conventional

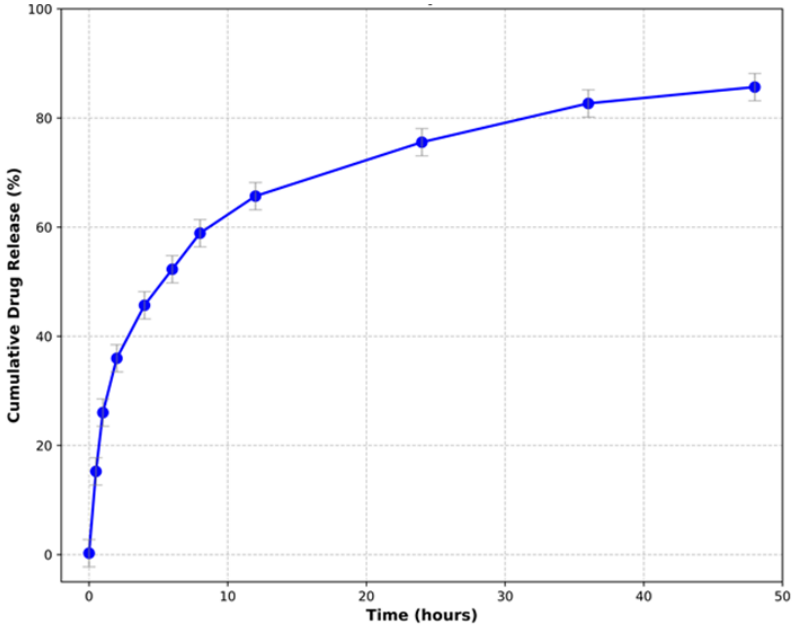

Fig. 6. *In vitro* release profile of ALA- loaded TPGS micelles.

nanocarriers of 45-60% encapsulation efficiency. For instance, the encapsulation efficiency of ALA in the chitosan nanoparticles was 62.4% [45]. The amphiphilic nature of the TPGs micellular system is underlying the high encapsulation efficiency of ALA in this ideal environment. However, the loading efficiency is a term used to describe the percentage of the nanocarrier loaded/occupied with/by the drug. Hence encapsulation efficiency and loading efficiency are interchangeable crucial terms in the context of drug delivery.

In Vitro Release Profile Analysis

The release of ALA from ALA-loaded TPGs micellular system, conducted over 48 hours under physiological conditions, revealed a biphasic release as elucidated in Fig. 6. ALA release showed an initial burst release, during the first 6 hours, of 52.4 ± 2.5% of the encapsulated amount followed by a sustained release period. The obtained release profile is well-consistent with the amphiphilic nature of the nanocarrier TPGs and the interactions between the vitamin E core of TPGs and the incorporated drug [46, 47]. The burst release could be derived from the ALA existing in the outer layers of TPGs or ALA with weak association with the nanocarrier corona. Similarly, Gorantla et al., observed 45-55% burst release of the drug from TPGs-based delivery system [48]. However, the sustained release period resulted in 75.8 ± 2.5 and 85.9 ± 2.5% ALA release after 24 and 48 hours, respectively as elucidated in Fig. 6. This sustainable release of ALA is considered an advantageous criterion to guarantee the availability of the drug delivery an extended period in biological systems and likelihood of dosage reduction [49].

FTIR Spectral Analysis

The molecular structure and potential interactions between TPGS and α-lipoic acid were deciphered using FTIR as elucidated in Fig. 7. The FTIR spectrum of TPGS, depicted in Fig. 7, exhibits characteristic absorption bands at distinctive wavelengths. Distinctive absorption bands observed at 3400 cm^{-1}, 2850-2950 cm^{-1}, and 1750 cm^{-1} correspond to the O-H stretching vibrations of the terminal hydroxyl groups, the C- H stretching vibrations of methylene groups present in both the PEG portion and the vitamin E component of TPGS, and the C=O stretching of the ester linkage, respectively, which are collectively

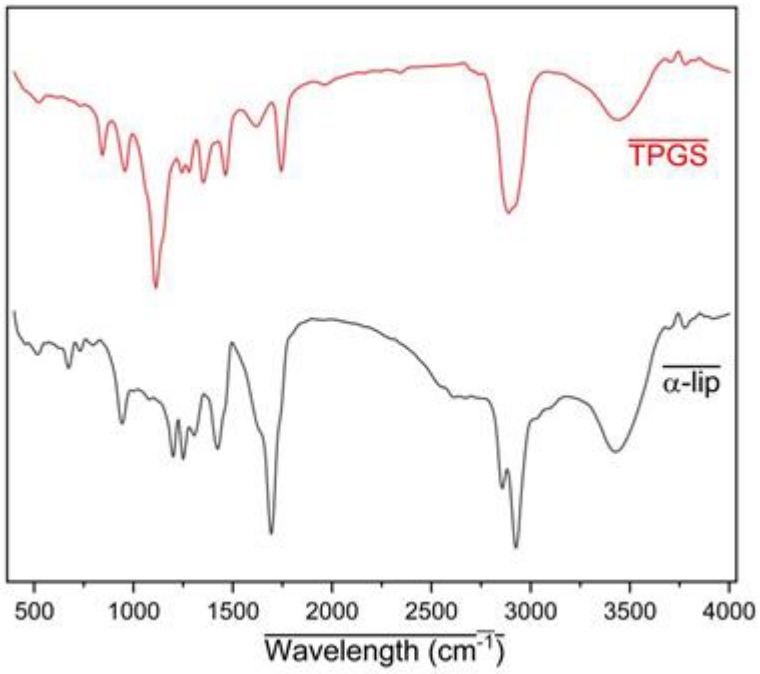

Fig. 7. FTIR profile of TPGS and ALA.

crucial features of TPGs structure [50, 51]. However, the FTIR spectrum, portrayed in Fig. 7, shows distinctive absorption peaks at 3000-3500 cm^{-1}, 1, 700 cm^{-1}, and 500-550 cm^{-1}region indicate the O-H stretching of the carboxylic acid group, the C=O stretching vibration of the carboxylic acid group, and the disulfide bond (-S-S-), respectively, which are together key features of ALA molecular structure [52].

Cell viability appraisal

The cytotoxicity of the ALA-loaded TPGs nanoparticles formulation was evaluated on human mesenchymal stem cells (Fig. 8). The results of MTT assay conferred a distinctive pattern of dose-dependent cell viability along with the concentration of the ALA-loaded TPGs. The cytotoxicity is directly proportional to the concentration of the ALA-loaded TPGs. Cell viability of 34.93±0.42, 48.36±0.51, 55.95±0.47, 85.78 ±0.33, and 85.90 ±0.97%, were observed at ALA-loaded TPGs concentrations of 100, 50, 25, 12.5, and 6.25%, respectively (Fig. 8). Data revealed substantial insights into the biocompatibility profile of the suggested delivery system ALA-loaded TPGs. In other words, an obvious threshold concentration of ALA-loaded TPGs nano-formulation of 6.25-12.5% was defined, accompanied with a superior cell biocompatibility described by a cell viability of approximately 85%. Present data could be explained on the basis of the amphiphilic nature of TPGs that would influence cell membrane integrity as elucidated previously [53]. Meanwhile, the relatively low concentration of the ALA-loaded TPGs nanoparticles would infer the safety therapeutic window to be exploited. The findings are mostly noteworthy for stem cell-based applications, where keeping cell viability is a critical aspect [54].

Characteristics of PLGA-ICAA nanoparticles

DLS and zeta potential pattern analysis

The DLS pattern settled in Fig. 9A revealed that the icariin-loaded PLGA nanoparticles showed a monomodal size distribution with a Z-average diameter and PDI of 469.1 nm and 0.234, respectively. The quite low PDI value (<0.3) evidences a rationally homogeneous size distribution, which is vital for keeping consistent drug release kinetics and cellular uptake patterns [55]. The remarkable particle size is superlative for well cell uptake and lengthy drug release, in accordance with previous findings [56]. Regarding the zeta potential measurements, a negative surface range of -1.2mV accompanied with a peak width of 4.88 mV was shown as elucidated in Fig. 9B. The negative value could be assigned to COO- groups in the PLGA polymer chains exposed on the surface of the nanoparticle. Meanwhile, the magnitude of the value is still low reflecting

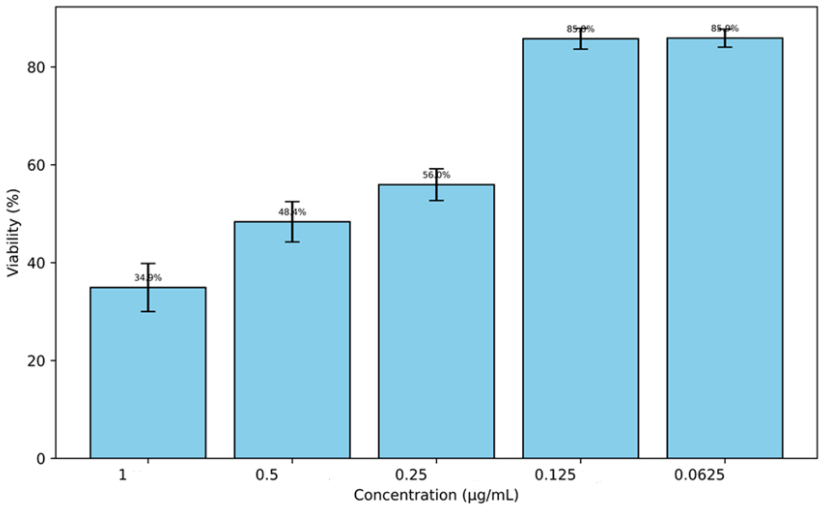

Fig. 8. Viability of human mesenchymal stem cells results at different concentration for ALA-loaded TPGS micelles formulation. Values are the average of three replicates ±SE.

the colloidal stability of the system through electrostatic repulsion. However, the narrow peak width confers the uniformity in surface charge distribution. Present finding is in a good agreement with those of Sivák *et al*. [57]. The moderate negative charge might help decrease the non-specific protein adsorption though keeping sufficient stability under physiological conditions [58]. Present finding regarding the DLS and zeta potential would evidence that the nano-formulation of icariin-loaded PGLA display excellent favorable pharmacokinetic properties and cellular interactions.

Morphological analysis by SEM

The morphological criteria of icariin-loaded PGLA nanoparticles were deciphered by Sem as shown in Fig. 10. Well-defined spherical nanoparticles with smooth surfaces lacking any irregularities or aggregations, a vital criterion for well-controlled drug delivery applications, were noted. This would in turn reflect the

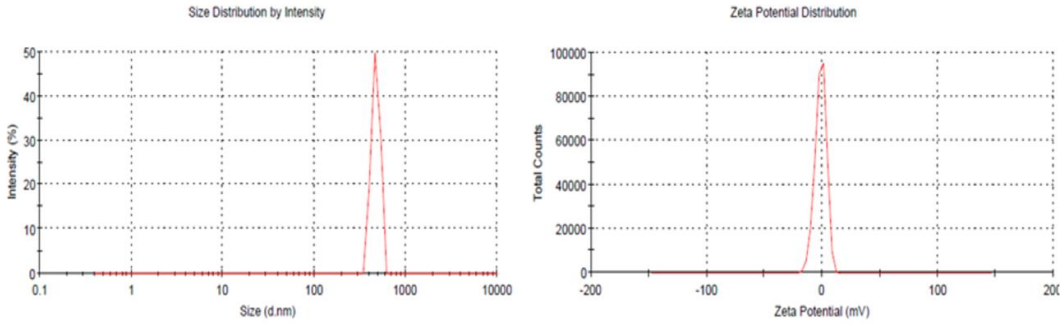

Fig. 9. DLS (A) and Zeta Potential (B) of PLGA nanoparticle.

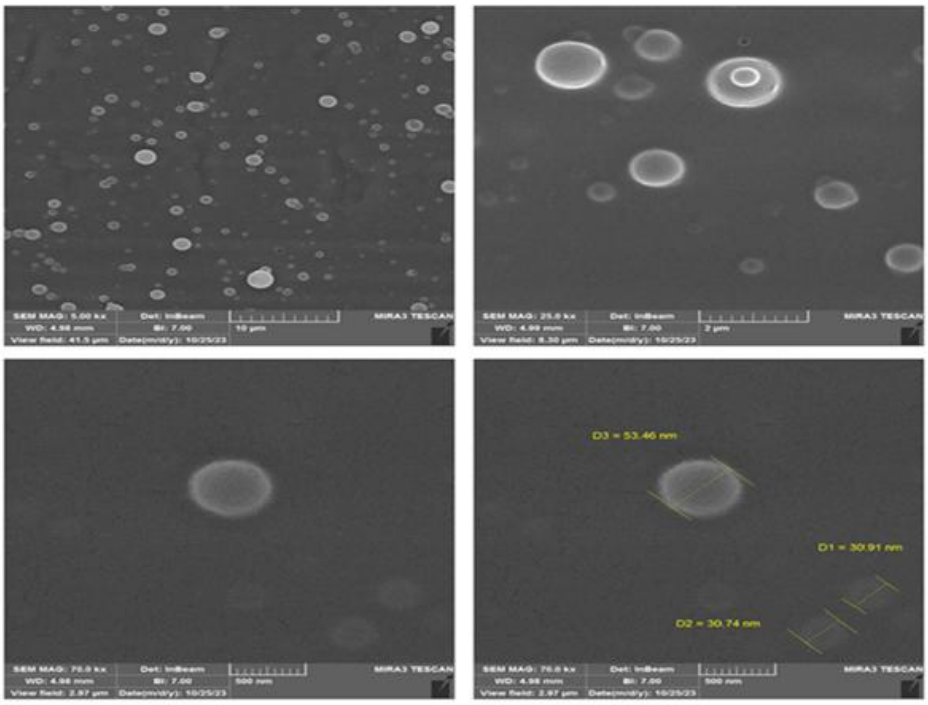

Fig. 10. SEM images of icariin-loaded PLGA nanoparticles picked up at different magnifications.

successful control over the emulsification-solvent evaporation process. The diameter of the spherical nanoparticles ranged from 30.0-55.0 nm, with majority of clustering around 39.6 nm. This would in turn the falling of the PLGA -based nanocarrier within the optimal window for enhanced cellular uptake and prolonged circulation time [27]. Successful evaporation of the organic solvents during the preparation processes an efficient drug encapsulation were evidenced by the appearance of smooth surfaces of the spherical nanoparticles. Present finding is in a well-agreement with the finding of Makadia and Siegel addressing the importance of surface characteristics in determining drug release patterns from PLGA nanoparticles [59]. The homogeneity in particle size would ascertain regular drug loading and release kinetics as previously reported [60].

Icariin Loading Analysis

The incorporation of icariin into PLGA nanoparticles was quantitatively appraised using a validated HPLC method. The HPLC chromatographic analysis for icariin-loaded PLGA revealed a well-resolved peak for the icariin-loaded PLGA nanoparticles (Fig. 11 B). Similarly, a well-resolved peaks was obtained for the standard icariin solution (Fig. 11A). The retention time for

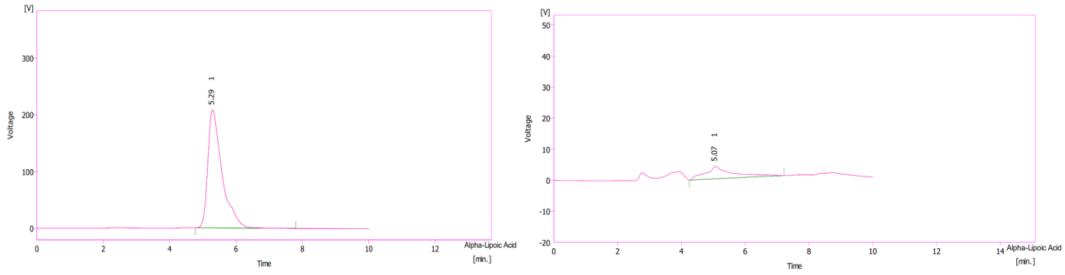

Fig. 11. HPLC chromatograms showing (A) icariin standard solution (100 µg/mL) with retention time at 5.09 minutes, and (B) drug-loaded PLGA nanoparticle extract demonstrating successful drug incorporation and method specificity.

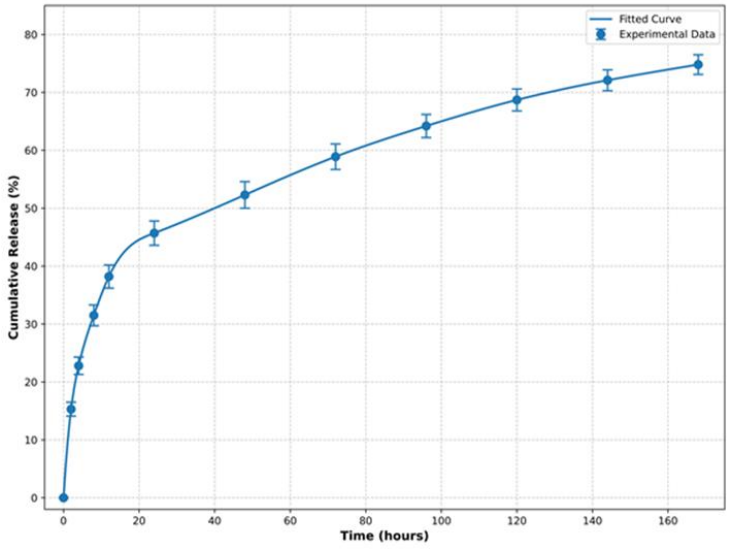

Fig. 12. *In vitro* release profile of icariin- loaded PLGA nanoparticles. Values are the average of three readings ±SE.

the icariin peak regardless its source (standard or nano-formula based loaded PLGA carrier), was approximately 5.09 minutes (Fig. 11). The symmetry of each peak and baseline stability underpin the robust separation, chromatograms demonstrate excellent peak symmetry and baseline stability, indicating robust separation conditions and minimal matrix interference from the PLGA carrier system. The drug loading content (DLC) achieved in our PLGA nanoparticle formulation was 7.0 ± 0.4%, representing a moderate loading capacity typical for hydrophilic drugs in PLGA matrices. The HPLC method demonstrated exceptional analytical performance across all critical parameters. The calibration curve exhibited excellent linearity (R^2>0.999) over the concentration range of 0.5-100 µg/ ml. The method's specificity is evidenced by the clean baseline and absence of interfering peaks in the chromatogram of drug-loaded nanoparticles (Fig. 11B), indicating effective separation of icariin from potential matrix components. The noted retention time of 5.09 minutes does allow for effective analysis and maintain good peak resolution, comparable to previously reported methods for icariin quantification.

Release Kinetics

A biphasic pattern characteristic of biodegradable polymeric system was obtained by icariin upon monitoring its release from the icariin-loaded PLGA nanoparticles in vitro (Fig. 12). An initial burst release of icariin followed by sustained release phase extending over 7 days. In the initial burst phase (24 hours), around 45.7 ± 2.1% of the encapsulated drug was released. This phenomenon can be assigned to the quick dissolution of surface-correlated or poorly entrapped drug molecules and the presence of drug molecules near the particle surface as well. The next sustained release phase exhibited or displayed a more gradual drug release pattern, realizing 74.8 ± 1.7% cumulative release by the seventh day. This prolonged sustained drug release period is co-matched with the nature of the biodegradable polymer PLGA where the drug diffusion occurs co-parallel with the polymer biodegradation. This sustained release adds an advantageous value for the release profile to guarantee prolonged drug concentration over an extended period in clinical applications. Similar finding was reported by Liu et al., where biphasic release patterns for hydrophilic compounds from

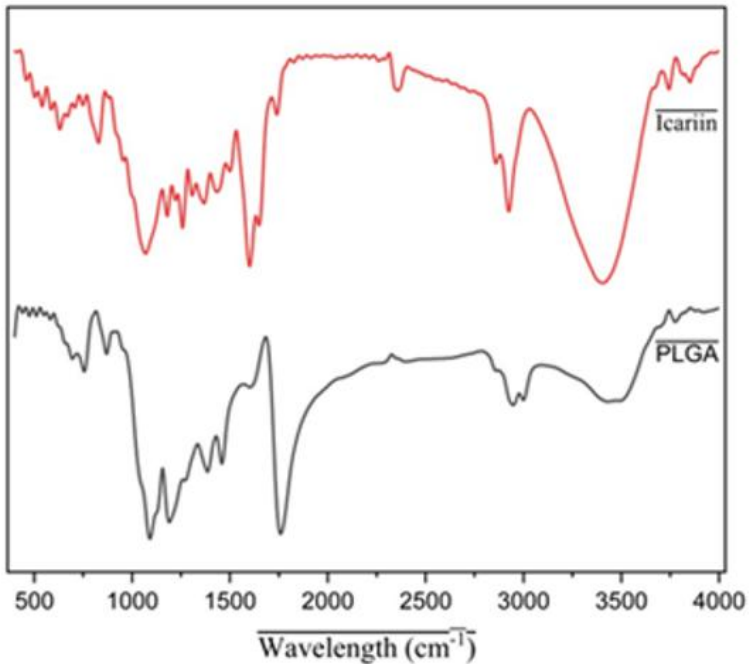

Fig. 13. FTIR spectra of icariin (red, top) and PLGA (black, bottom).

PLGA nanoparticles, with 40-50% in the burst initial period realizing sustained release period from 7-10 days [61].

FTIR spectral analysis

The FTIR spectral analysis demonstrates substantial information about the molecular structure and interactions within the icariin-loaded PLGA nanoparticle system (Fig. 13). In the PLGA spectrum, the characteristic strong absorption band at approximately 1750 cm^{-1}, corresponds to the C=O stretching vibration of the ester groups. This finding is in agreement with other findings settled in previous studies [59], stated that this peak is peculiar for the PLGA polymer. Other characteristics PLGA peaks appeared appeared at 2995 cm^{-1} (CH stretch) and 1450 cm^{-1} (CH3 asymmetric deformation), reliable with previous findings [62].

The pure icariin spectrum demonstrates typical absorption bands that correspond to its molecular structure, specifically the broad band at 3400 cm^{-1} (O-H stretching vibrations) and peaks at 2925 cm^{-1} (C-H stretching). These spectral features are in a good accordance with those reported by Ma et al. in their detailed characterization of icariin [63]. The presence of peaks at 1650 cm^{-1} (C=O stretching) and 1610 cm^{-1} (aromatic C=C stretching) further verifies the flavonoid structure of icariin.

Cells Viability Analysis

The cytotoxicity evaluation of icariin-loaded PLGA nanoparticles on human mesenchymal stem cells reflected excellent biocompatibility across all studied concentrations. The cell viability profile (Fig. 14) demonstrated a partial concentration-dependent pattern, with all concentrations maintaining high cell viability above 89%. At the highest concentration (100%), the mean cell viability was 89.70± 0.56%, indicating minimal cytotoxicity even at maximum exposure. As the concentration decreased, cell viability showed a gradual increase, with the lowest concentration (6.25%) exhibiting the highest viability of 99.05 ± 0.39% (Fig. 14). The partial dose-dependent response noted in our study did align with previous findings by Wang et al., who reported similar biocompatibility patterns for PLGA-based nanocarrier systems [64]. The high cell viability (>95%) observed at concentrations of 50% and below suggests a wide therapeutic window for potential clinical applications.

The minimal cytotoxicity can be attributed to several factors, such as the biodegradable nature of PLGA polymer, controlled release properties of the nanoparticle system, and inherent biocompatibility of icariin. These results suggest that icariin-loaded PLGA nanoparticles are safe for cellular applications within the tested concentration range, making them promising candidates for therapeutic applications. The high cell viability even at 100% concentration indicates a potentially broad therapeutic window for future *in vivo* applications.

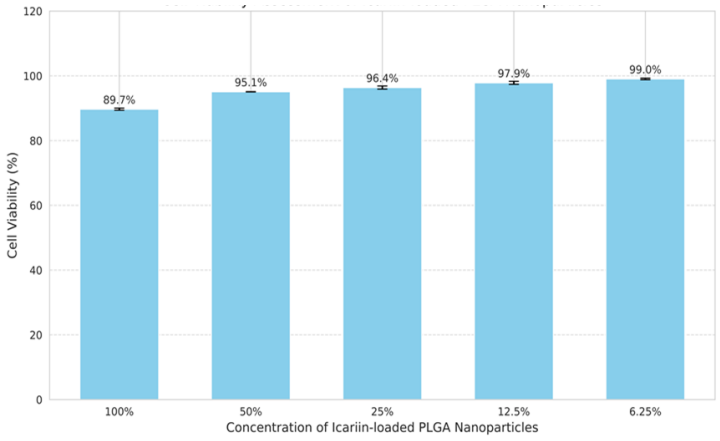

Fig. 14. Cell Viability Assessment of icariin-loaded PLGA nanoparticles.

CONCLUSION

This study successfully established and characterized a highly promising hydrogel biocomposite system for bone tissue engineering. The optimum formulation, comprising a 4:12:6 ratio of methylcellulose, gelatin, and sodium alginate, demonstrated robust mechanical characteristics, further enhanced by 0.5% graphene oxide incorporation. The study also achieved efficacious synthesis and characterization of two discrete nano-formulations: ALA-loaded TPGs micelles and icariin-loaded PLGA nanoparticles. Both nanocarrier systems displayed ideal criteria for drug delivery, including satisfactory particle size and surface charge, promising drug encapsulation efficiency, and sustained release patterns over prolonged periods. These results collectively confirm that the fabricated hydrogel composite, harboring these drug-loaded nanocarriers, represents a highly suitable and viable platform for targeted and prolonged delivery of osteo-regenerative agents, paving the way for enhanced bone regeneration and repair.

ACKNOWLEDGEMENT

The authors would like to thank an AI language model for its assistance with English editing of this manuscript.

CONFLICT OF INTEREST

The authors declare that there is no conflict of interest regarding the publication of this manuscript.

REFERENCES

1. Wang Y-M, Shen J-T. Chitosan-based promising scaffolds for the construction of tailored nanosystems against osteoporosis: Current status and future prospects. Journal of Applied Biomaterials and Functional Materials. 2024;22.
2. Zhang P, Qi J, Zhang R, Zhao Y, Yan J, Gong Y, et al. Recent advances in composite hydrogels: synthesis, classification, and application in the treatment of bone defects. Biomaterials Science. 2024;12(2):308-329.
3. Batool M, Abid MA, Javed T, Haider MN. Applications of biodegradable polymers and ceramics for bone regeneration: a mini-review. International Journal of Polymeric Materials and Polymeric Biomaterials. 2024;74(1):39-53.
4. Brückner T, Gbureck U. Nano-magnesium phosphate hydrogels: efficiency of an injectable and biodegradable gel formulation towards bone regeneration. AME Medical Journal. 2017:51-51.
5. Xin W, Gao Y, Yue B. Recent Advances in Multifunctional Hydrogels for the Treatment of Osteomyelitis. Frontiers in Bioengineering and Biotechnology. 2022;10.
6. Synthesis of Poly(methacrylic acid)/Montmorillonite Hydrogel Nanocomposite for Efficient Adsorption of Amoxicillin and Diclofenac from Aqueous Environment: Kinetic, Isotherm, Reusability and Thermodynamic Investigations. American Chemical Society (ACS).
7. Yang C, Wu T, Qi Y, Zhang Z. Recent Advances in the Application of Vitamin E TPGS for Drug Delivery. Theranostics. 2018;8(2):464-485.
8. Qu H, Fu H, Han Z, Sun Y. Biomaterials for bone tissue engineering scaffolds: a review. RSC Advances. 2019;9(45):26252-26262.
9. Jia B, Huang H, Dong Z, Ren X, Lu Y, Wang W, et al. Degradable biomedical elastomers: paving the future of tissue repair and regenerative medicine. Chem Soc Rev. 2024;53(8):4086-4153.
10. Tibbitt MW, Anseth KS. Hydrogels as extracellular matrix mimics for 3D cell culture. Biotechnology and Bioengineering. 2009;103(4):655-663.
11. Yi J, Choe G, Park J, Lee JY. Graphene oxide-incorporated hydrogels for biomedical applications. Polym J. 2020;52(8):823-837.
12. Wu Y, Zhang X, Zhao Q, Tan B, Chen X, Liao J. Role of Hydrogels in Bone Tissue Engineering: How Properties Shape Regeneration. J Biomed Nanotechnol. 2020;16(12):1667-1686.
13. N. Zghair A, T. Al-Khateeb Z, S. Jasim L, Batool M. Synthesis, characterization and adsorption properties of azo-functionalized polymeric hydrogels for R6G dye removal from water. Applied Chemical Engineering. 2025;8(1).
14. El-Say KM, Ahmed OAA, Mohamed AI, Safo MK, Omar ASM. and Zein-alpha lipoic acid-loaded nanoparticles to enhance the oral bioavailability of dapoxetine: optimization and clinical pharmacokinetic evaluation and International Journal of Nanomedicine. 2019;Volume 14:7461-7473.
15. Mehata AK, Setia A, Vikas V, Malik AK, Hassani R, Dailah HG, et al. Vitamin E TPGS-Based Nanomedicine, Nanotheranostics, and Targeted Drug Delivery: Past, Present, and Future. Pharmaceutics. 2023;15(3):722.
16. Shen X, Yu P, Chen H, Wang J, Lu B, Cai X, et al. Icariin controlled release on a silk fibroin/mesoporous bioactive glass nanoparticles scaffold for promoting stem cell osteogenic differentiation. RSC Advances. 2020;10(20):12105-12112.
17. Mohammadzadeh M, Zarei M, Abbasi H, Webster TJ, Beheshtizadeh N. Promoting osteogenesis and bone regeneration employing icariin-loaded nanoplatforms. J Biol Eng. 2024;18(1).
18. Han X, Chang S, Zhang M, Bian X, Li C, Li D. Advances of Hydrogel-Based Bioprinting for Cartilage Tissue Engineering. Frontiers in Bioengineering and Biotechnology. 2021;9.
19. Cui X, Li J, Hartanto Y, Durham M, Tang J, Zhang H, et al. Advances in Extrusion 3D Bioprinting: A Focus on Multicomponent Hydrogel-Based Bioinks. Advanced Healthcare Materials. 2020;9(15).
20. Allahbakhsh A, Mazinani S, Kalaee MR, Sharif F. Cure kinetics and chemorheology of EPDM/graphene oxide nanocomposites. Thermochim Acta. 2013;563:22-32.
21. Patel KD, Singh RK, Kim H-W. Carbon-based nanomaterials as an emerging platform for theranostics. Materials Horizons. 2019;6(3):434-469.
22. Zhang J, Eyisoylu H, Qin X-H, Rubert M, Müller R. 3D bioprinting of graphene oxide-incorporated cell-laden bone mimicking scaffolds for promoting scaffold fidelity, osteogenic differentiation and mineralization. Acta Biomater. 2021;121:637-652.
23. Kosowska K, Korycka P, Jankowska-Snopkiewicz K, Gierałtowska J, Czajka M, Florys-Jankowska K, et al.

Graphene Oxide (GO)-Based Bioink with Enhanced 3D Printability and Mechanical Properties for Tissue Engineering Applications. Nanomaterials. 2024;14(9):760.
24. Habib MA, Khoda B. Rheological analysis of bio-ink for 3D bio-printing processes. Journal of Manufacturing Processes. 2022;76:708-718.
25. Di Giuseppe E, Davaille A, Mittelstaedt E, François M. Rheological and mechanical properties of silica colloids: from Newtonian liquid to brittle behaviour. Rheol Acta. 2012;51(5):451-465.
26. Georgieva S, Voyslavov T, Chanev C, Petrov O. Figure 1 from: Georgieva S, Voyslavov T, Chanev C, Petrov O (2025) High-performance liquid chromatography-based evaluation of lipophilicity of a series of novel stilbene derivatives. Pharmacia 72: 1-8. https://doi.org/10.3897/pharmacia.72.e141364. Pensoft Publishers; 2025.
27. Danhier F, Ansorena E, Silva JM, Coco R, Le Breton A, Préat V. PLGA-based nanoparticles: An overview of biomedical applications. Journal of Controlled Release. 2012;161(2):505-522.
28. Siepmann J, Siepmann F. Mathematical modeling of drug delivery. Int J Pharm. 2008;364(2):328-343.
29. Goldstein JI, Newbury DE, Michael JR, Ritchie NWM, Scott JHJ, Joy DC. Secondary Electrons. Scanning Electron Microscopy and X-Ray Microanalysis: Springer New York; 2017. p. 29-37.
30. Batool M, Haider MN, Javed T. Applications of Spectroscopic Techniques for Characterization of Polymer Nanocomposite: A Review. Journal of Inorganic and Organometallic Polymers and Materials. 2022;32(12):4478-4503.
31. Pandao MR, Sajid M. Assessing the impact of nano zinc oxide on growth, yield, and nutrient uptake by linseed. Journal of Natural Resource Conservation and Management. 2023;4(2):116-122.
32. Lee DY. Gelatin Enhances the Wet Mechanical Properties of Poly(D,L-Lactic Acid) Membranes. Int J Mol Sci. 2024;25(9):5022.
33. Moncada D, Bouza R, Rico M, Rodríguez-Llamazares S, Pettinelli N, Aragón-Herrera A, et al. Injectable Carrageenan/Green Graphene Oxide Hydrogel: A Comprehensive Analysis of Mechanical, Rheological, and Biocompatibility Properties. Polymers. 2024;16(16):2345.
34. Temirel M, Dabbagh SR, Tasoglu S. Shape Fidelity Evaluation of Alginate-Based Hydrogels through Extrusion-Based Bioprinting. Journal of Functional Biomaterials. 2022;13(4):225.
35. Benavente C, Romero A, Napa J, Sanabria A, Landivar Y, La Borda L, et al. The Influence of Graphene Oxide on the Performance of Concrete: A Quantitative Analysis of Mechanical and Microstructural Properties. Buildings. 2025;15(7):1082.
36. Liu T, Lu Y, Zhan R, Qian W, Luo G. Nanomaterials and nanomaterials-based drug delivery to promote cutaneous wound healing. Adv Drug Del Rev. 2023;193:114670.
37. Ouyang L, Highley CB, Sun W, Burdick JA. A Generalizable Strategy for the 3D Bioprinting of Hydrogels from Nonviscous Photo-crosslinkable Inks. Adv Mater. 2016;29(8).
38. Vishvanathperumal S, Kannan A. Effect of graphene oxide (GO) on the mechanical properties of ethylene-propylene-diene monomer/acrylonitrile butadiene rubber (EPNBR) blend composites. Journal of Polymer Research. 2025;32(4).
39. Nadernezhad A, Khani N, Skvortsov GA, Toprakhisar B, Bakirci E, Menceloglu Y, et al. Multifunctional 3D printing of heterogeneous hydrogel structures. Sci Rep. 2016;6(1).
40. Mitchell MJ, Billingsley MM, Haley RM, Wechsler ME, Peppas NA, Langer R. Engineering precision nanoparticles for drug delivery. Nature Reviews Drug Discovery. 2020;20(2):101-124.
41. Jin M, Nam JH, Na Y-G, Yun T-S, Song B, Hwang Y-R, et al. Enhanced Delivery of Sorafenib for Hepatocellular Carcinoma Treatment: Surface Modified PLGA Nanoparticles with Biomimetic Alterations. Elsevier BV; 2024.
42. Binkhathlan Z, Ali R, Alomrani AH, Abul Kalam M, Alshamsan A, Lavasanifar A. Role of Polymeric Micelles in Ocular Drug Delivery: An Overview of Decades of Research. Mol Pharm. 2023;20(11):5359-5382.
43. Lim SH, Wong TW, Tay WX. Overcoming colloidal nanoparticle aggregation in biological milieu for cancer therapeutic delivery: Perspectives of materials and particle design. Advances in Colloid and Interface Science. 2024;325:103094.
44. Tiwold EK, Gyorgypal A, Chundawat SPS. Recent Advances in Biologic Therapeutic N-Glycan Preparation Techniques and Analytical Methods for Facilitating Biomanufacturing Automation. J Pharm Sci. 2023;112(6):1485-1491.
45. Rosales-Martínez P, Garcia-Pinilla S, Arroyo-Maya IJ, Hernández-Sánchez H, Cornejo-Mazón M. Optimization of the conditions for the elaboration of chitosan nanoparticles charged with alpha lipoic acid, ascorbic and alpha-tocopherol. Revista Mexicana de Ingeniería Química. 2016;16(1):319-335.
46. Mohamed Saliq A, Krishnaswami V, Janakiraman K, Kandasamy R. α-Lipoic acid nanocapsules fortified cow milk application as a dietary supplement product for anemia. Applied Nanoscience. 2020;10(6):2007-2023.
47. Yi Y, Yu M, Li W, Zhu D, Mei L, Ou M. Vaccine-like nanomedicine for cancer immunotherapy. Journal of Controlled Release. 2023;355:760-778.
48. Gorantla S, Rao Puppala E, Naidu VGM, Saha RN, Singhvi G. Design of chondroitin sulphate coated proglycosomes for localized delivery of tofacitinib for the treatment of rheumatoid arthritis. Eur J Pharm Biopharm. 2023;186:43-54.
49. Bussing D, Li Y, Guo L, Verma A, Sullivan JM, Shah DK. Pharmacokinetics of Monoclonal Antibody and Antibody Fragments in The Mouse Eye Following Intravitreal Administration. J Pharm Sci. 2023;112(8):2276-2284.
50. Sunoqrot S, Aliyeh S, Abusulieh S, Sabbah D. Vitamin E TPGS-Poloxamer Nanoparticles Entrapping a Novel PI3Kα Inhibitor Potentiate Its Activity against Breast Cancer Cell Lines. Pharmaceutics. 2022;14(9):1977.
51. Yusuf O, Ali R, Alomrani AH, Alshamsan A, Alshememry AK, Almalik AM, et al. Design and Development of D–α–Tocopheryl Polyethylene Glycol Succinate–block–Poly(ε-Caprolactone) (TPGS–b–PCL) Nanocarriers for Solubilization and Controlled Release of Paclitaxel. Molecules. 2021;26(9):2690.
52. Xie D-M, Zhong Q, Xu X, Li Y, Chen S, Li M, et al. Alpha lipoic acid–loaded electrospun fibrous patch films protect heart in acute myocardial infarction mice by inhibiting oxidative stress. Int J Pharm. 2023;632:122581.
53. Kumari L, Singh R, Patel P, Singh A, Singh D, Sharma N, et al. QbD assisted development of hyaluronic acid and TPGS incorporated DOX liposome(s): in vitro assessment of cytotoxicity, uptake, ROS, and NF-κB potential on MDA-MB-231 cells. Naunyn-Schmiedeberg's Arch Pharmacol. 2025.
54. Lu J, Yang X, He C, Chen Y, Li C, Li S, et al. Rejuvenation of tendon stem/progenitor cells for functional tendon regeneration through platelet-derived exosomes loaded

with recombinant Yap1. Acta Biomater. 2023;161:80-99.
55. Jungebluth P, Haag JC, Lim ML, Lemon G, Sjöqvist S, Gustafsson Y, et al. Retraction notice to:"Verification of cell viability in bioengineered tissues and organs before clinical transplantation " [BIOMATERIALS (2013) 4057-4067]. Biomaterials. 2019;199:88.
56. N'Guessan Gnaman KC, Bouttier S, Yeo A, Aka Any-Grah AAS, Geiger S, Huang N, et al. Characterization and in vitro evaluation of a vaginal gel containing Lactobacillus crispatus for the prevention of gonorrhea. Int J Pharm. 2020;588:119733.
57. Sivák L, Šubr V, Kovářová J, Dvořáková B, Šírová M, Říhová B, et al. Polymer-ritonavir derivate nanomedicine with pH-sensitive activation possesses potent anti-tumor activity in vivo via inhibition of proteasome and STAT3 signaling. Journal of Controlled Release. 2021;332:563-580.
58. Long Q, Zheng P, Zheng X, Li W, Hua L, Yang Z, et al. Engineered bacterial membrane vesicles are promising carriers for vaccine design and tumor immunotherapy. Adv Drug Del Rev. 2022;186:114321.
59. Makadia HK, Siegel SJ. Poly Lactic-co-Glycolic Acid (PLGA) as Biodegradable Controlled Drug Delivery Carrier. Polymers. 2011;3(3):1377-1397.
60. Kamaly N, Yameen B, Wu J, Farokhzad OC. Degradable Controlled-Release Polymers and Polymeric Nanoparticles: Mechanisms of Controlling Drug Release. Chem Rev. 2016;116(4):2602-2663.
61. Liu Q, Wei F, Coathup M, Shen W, Wu D. Effect of Porosity and Pore Shape on the Mechanical and Biological Properties of Additively Manufactured Bone Scaffolds. Advanced Healthcare Materials. 2023;12(30).
62. Feczkó T, Tóth J, Gyenis J. Comparison of the preparation of PLGA–BSA nano- and microparticles by PVA, poloxamer and PVP. Colloids Surf Physicochem Eng Aspects. 2008;319(1-3):188-195.
63. Ma H, He X, Yang Y, Li M, Hao D, Jia Z. The genus Epimedium: An ethnopharmacological and phytochemical review. J Ethnopharmacol. 2011;134(3):519-541.
64. Han G-Y, Hwang S-K, Cho K-H, Kim H-J, Cho C-S. Progress of tissue adhesives based on proteins and synthetic polymers. Biomaterials Research. 2023;27(1).